Organic Electronics 9 (2008) 1069–1075

Contents lists available at ScienceDirect

Organic Electronics

journal homepage: www.elsevier.com/locate/orgel

Controllable carrier density of pentacene field-effect transistors using polyacrylates as gate dielectrics

Jung-An Cheng *, Chiao-Shun Chuang, Ming-Nung Chang, Yan-Chu Tsai, Han-Ping D. Shieh

Department of Photonics and Display Institute, National Chiao Tung University, Rm. 501 CPT Building, 1001 Ta Hsueh Road, Hsinchu 30010, Taiwan

ARTICLE INFO

Article history:
Received 2 May 2008
Received in revised form 5 August 2008
Accepted 11 August 2008
Available online 19 August 2008

PACS:
52.25.Mq
61.66.Hq
61.82.Fk
61.82.Ms
61.82.Pv
68.47.Mn

Keywords:
OTFT
Polyacrylate
Pentacene
PMMA
Dielectric

ABSTRACT

We have studied the effect of the chemical structure of dielectrics by evaporating pentacene onto a series of polyacrylates: poly(methylmethacrylate), poly(4-methoxyphenylacrylate), poly(phenylacrylate), and poly(2,2,2-trifluoroethyl methacrylate) in organic thin-film transistors (OTFTs). In top-contact OTFTs, the polyacrylates had a significant effect on field-effect mobilities ranging $0.093 \sim 0.195$ $cm^2 V^{-1} s^{-1}$. This variation neither correlated with the polymer surface morphology nor the observed pentacene crystallite size. This result implies that the PTFMA device generates the local electric field that accumulates holes and significantly shifts the threshold voltage and the turn-on voltage to −8.62 V and 3.5 V, respectively, in comparison with those of PMMA devices.

1. Introduction

Ever since the first organic thin-film transistors (OTFTs) based on polymer [1–3] and small molecule [4,5] semiconductors were reported, interest in this field has risen steadily for both technological and scientific reasons. OTFTs are of interest for a variety of electronic applications, such as radio frequency identification (RFID) tags [6], flexible display [6,7], sensors [8], and electronic barcodes [9,10]. Prototypes of these products have been demonstrated and are now gearing towards commercialization.

Recent technological advances in OTFTs have triggered intensive research into the molecular and mesoscale structures of organic semiconductor films that determine their charge transport characteristics. Since the molecular structure and morphology of an organic semiconductor are largely determined by the properties of the interface between the organic film and dielectric, a great deal of research has focused on interface engineering. Kobayashi et al. [11], have reported that self-assembled monolayers (SAMs) accumulate holes in the transistor channel. These properties can be understood in terms of the effects of the electric dipoles of SAM molecules, and weak charge transfer between organic films and SAMs. The technique provides a simple way of controlling channel charge density and thus also the threshold voltage at low density levels, which should be of useful for fabricating OTFTs with improved functionality [12].

Polymeric insulators have been considered as preferable gate dielectric materials, in part, because films exhibiting good characteristics can often be formed simply by

* Corresponding author. Tel.: +886 3 5712121x59210; fax: +886 3 5737681.
E-mail address: jacheng.ac89g@nctu.edu.tw (J.-A. Cheng).

1566-1199/$ - see front matter © 2008 Elsevier B.V. All rights reserved.
doi:10.1016/j.orgel.2008.08.004

spin-coating, casting, or printing at room temperature and under ambient conditions. The mobility of the most pentacene-based OTFTs is significantly influenced and dominated by characteristics of applied gate dielectrics. PMMA is a well-known glasslike material in photonics [13]. Recently, PMMA used as a gate dielectric layer in OTFTs is also being considered, because of it shows not only good output and transfer characteristics but also potential to alternate SiO_2 as the gate dielectric in OTFTs [14–17].

In this paper, we present the study of the field-effect on pentacene-based organic TFT by using polyacrylates as dielectric layers. To control channel conductance and carrier density without using gate voltage, a series of dipole tunable polyacrylates, which are derived from PMMA matrix, are investigated as dielectric layers. By using pentacene-based OTFTs with a top-contact configuration, we will also characterize the dipole effect on the semiconductor/dielectric interface. The output and transfer characteristics related to carrier density, including field-effect mobility (μ_{sat}), on-off current ratio (I_{on}/I_{off}), turn-on voltages (V_{on}), and threshold voltages (V_{Th}), were also examined.

2. Experimental

All of the materials used in the experiment were commercially available, and solvents were used without further purification. The purity of gold and aluminum metal are 99.8%. The molecular weight of commercial poly(methylmethacrylate) (PMMA) is 15,000 g/mol. Poly(phenylacrylate)[18], poly(4-methoxyphenylacrylate) (PMPA)[19], and poly(2,2,2-trifluoroethyl methacrylate) (PTFMA)[20] were prepared according to the references. Thermal decomposition temperature (T_d), glass transition temperature (T_g), and molecular weight (M_w) of polyacrylates were determined by thermogravimetric analysis (TGA, SEIKO I TG/DTA 200), differential scanning calorimetry (DSC, SEIKO SII DSC 2000), and a Water 600 gel permeation chromatography (GPC), respectively. Surface affinity of polyacrylates thin-films was measured by using a Paul N. Gardner contact angle detector.

2.1. Device fabrication

The patterned ITO glass substrates were cleaned ultrasonically with detergent, deionized water, 2-propanol, and methanol, followed by UV-ozone pretreatment before use. For top-contact OTFTs fabrication, polyacrylates were dissolved in toluene with 12.0 wt%, spin-coated onto ITO substrates at 1000 rpm for 30 s, and dried in a vacuum oven at 80 °C for 4 h. Thereafter, pentacene was thermally deposited at 6×10^{-6} Torr (ca. 0.3–0.4 Å s^{-1}) with a film thickness of 600 Å. Top-contact Au electrodes (ca. 70 nm) were then deposited through a shadow mask. The channel length (L) and width (W) of the devices were 200 and 2000 μm, respectively. The film thickness and roughness were measured using a DI 3100 atomic force microscopy (AFM). The current–voltage (I–V) characteristics of OTFTs were measured using a Keithley 4200 semiconductor parameter analyzer and a HP 4284 CV analyzer.

3. Result and discussion

3.1. Characterization of gate dielectric surface

To investigate the effect of polyacrylates gate dielectrics on pentacence-based OTFTs, a series of polyacrylates with different ester substitutes (4-methoyxphenyl (PMPA), phenyl (PPA), and 2,2,2-trifluoroethyl (PTFMA) side chain

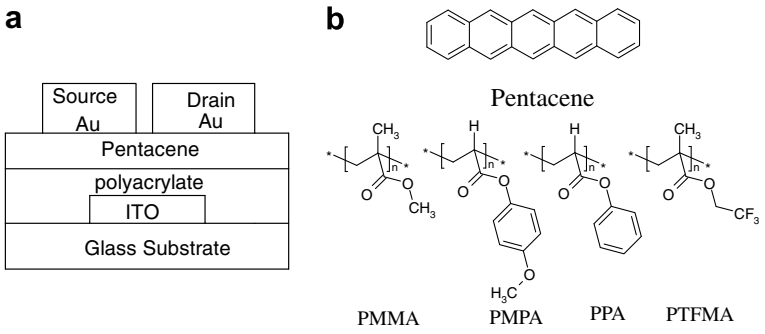

Fig. 1. (a) The schematic of top-contact OTFT and (b) chemical structures of materials used in this study.

Table 1
Gate dielectric thin-film surface characteristics

Dielectric material	T_g (°C)	Thickness (nm)	Surface roughness (R_a; nm)	Surface contact angle (°)[a]	Surface free energy (SFE; mJ m^{-2})	Dielectric constant (k)[b]
PMMA	105.2	560	0.32	74	38.19	3.2
PMPA	133.2	660	0.40	75	37.54	3.4
PPA	135.7	582	0.20	90	27.91	2.9
PTFMA	82.4	592	0.44	95	24.75	6.0

[a] Measured by using DI-water droplets.
[b] Measured at 1.0 kHz.

groups) were synthesized. Their corresponding chemical structures and the OTFT configuration are depicted in Fig. 1.

The dielectric thermal properties and thin-film surface were characterized and summarized in Table 1. In thermal analysis, both PMPA and PPA show higher T_g than that of PMMA and PTFMA, implying the rigidity of the side-chain group. All dielectrics had comparable thickness (560–660 nm) were spin-cast, and exhibited very similar topologies. The deposited dielectric thin-films were observed to be pinhole-free and smooth; whose root-mean-square roughness was within 0.20–0.44 nm.

Improved mobility could be depicted by changes in the surface energy of gate dielectrics [21]. In addition, lowering the surface energy on a gate dielectric was identified as a key factor to increasing the grain size during the growth of pentacene. To evaluate those parameters related to the thin-film surface free energy (SFE), we utilize Eq. (1), obtained from both Young's equation and the equation of state for solid/liquid interfacial tension, to estimate the surface free energy (SFE) of gate dielectrics [22].

$$\gamma_L(1+\cos\theta) = 2(\gamma_L\gamma_s)^{1/2} e^{-\beta(\gamma_L-\gamma_s)^2}, \quad (1)$$

where γ_L, γ_s, θ, and β is the surface tension of water, the surface energy of the solid, the measured contact angle, and an empirical constant with an average value of 1.06×10^{-4} $(m^2\ mJ^{-1})^2$, respectively. In estimating surface energy γ_s, the surface tension of water is substantially adopted as 72.88 mJ/m^2.

The surface contact angle of polyacrylates and their corresponding SFE, which were calculated according to Eq. (1), summarized in Table 1, are dominated by the hydrophobicity of ester groups SFE also decreases with increasing the surface contact angle. In structural modification, dielectric constant (k) is substantially increased for PMPA and PTFMA while high polar substitutes instead of methyl groups in ester linkage. The dielectric constants of PPA, PMMA, PMPA, and PTFMA were obtained as 2.9, 3.2, 3.4,

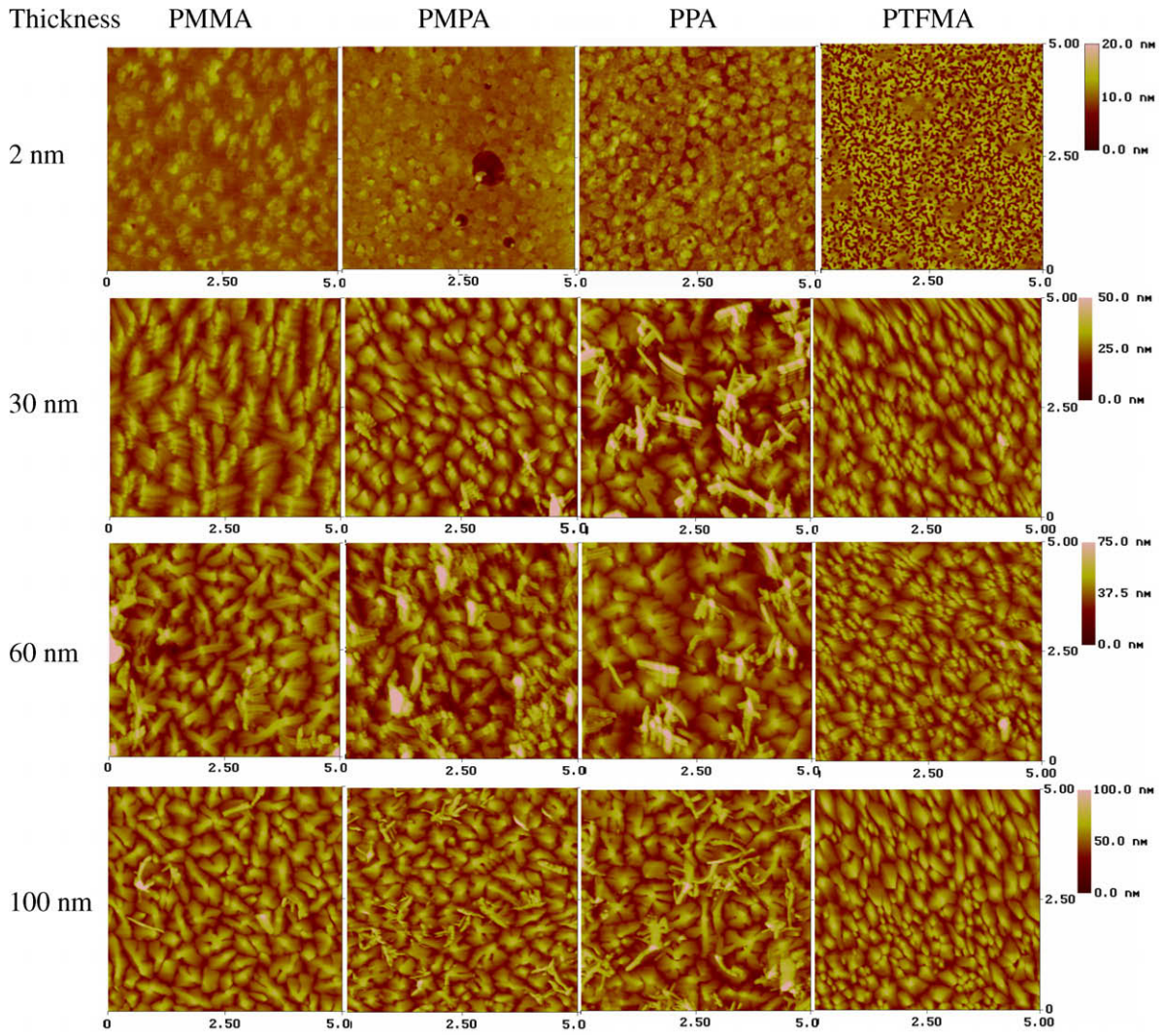

Fig. 2. AFM images of pentacene films grown on various dielectric substrates: (a) PMMA, (b) PMPA, (c) PPA and (d) PTFMA.

and 6.0, respectively. The measured k value of PTFMA is extremely high, owing to the electronegative characteristic of the 2,2,2-trifluoroethyl group.

3.2. Topography of pentacene thin-film

To study thin-film growth mechanisms during the thermal evaporation process, we utilized the AFM to measure the surface morphology of pentacenes of 2, 30, 60, and 100 nm in thickness. The profiles were measured in the channel region and are shown in Fig. 2, where grain size increases with film thickness, the grain shape is independent of pentacene film thickness. Although the surface morphology of pentacene is measured on different polyacrylate dielectrics, the typical crystallites size is remarkably similar, roughly 0.3–0.7 μm, as shown in Fig. 2. This fact is also found that the pentacene film growth mode/morphology variations are closely correlated with the surface energy of the corresponding polymer substrates. Different semiconductor film growth mechanisms are involved with different dielectric substrates, which can be associated with either formal Frank-van der Merwe (layer-by-layer) or Volmer-Weber (island) growth modes [23]. The needle-like growths, visible in the images of PMMA, PMPA, and PPA are most likely pentacene dihydride [24]. Most of the substrates show crystallites of the usual dendritic form, and their corresponding pentacene growth mechanisms show as layer-by-layer growth modes. However, the growth mechanism of PTFMA is totally different from that of mentioned above. The dendritic feature is not observed in PTFMA substrate. What displaces are dense grains with island growth mode, implying that the crystal growth of the first seeding of pentacene on the flat substrate was significantly affected when the dielectric surface energy relatively approaches to that of surface energy on pentacene crystal plane [25,26].

3.3. The output and transfer characteristics of OTFTs

The output characteristics (I_{DS} vs. V_{DS}) with various gate voltages (V_{GS}) for pentacene TFTs using polyacrylates as the gate insulator are plotted in Fig. 3. All devices show good saturation characteristics as a drain-source bias. The I_{DS}–V_{DS} output characteristics show a p-channel accumulation type field-effect transistor. Under a given gate voltage V_{GS}, the device with PTFMA gate dielectric shows similar

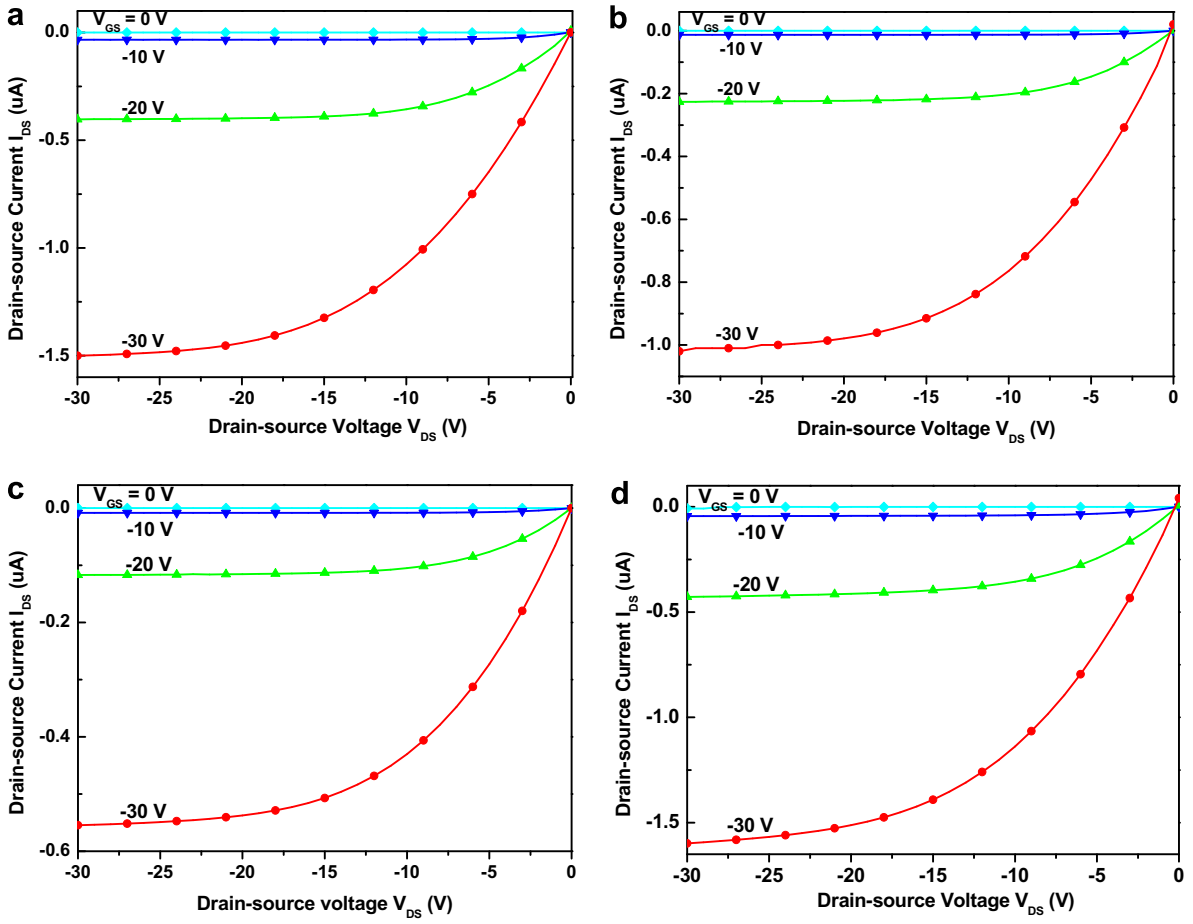

Fig. 3. Output characteristics of OTFTs with different gate dielectrics: (a) PMMA, (b) PMPA, (c) PPA and (d) PTFMA.

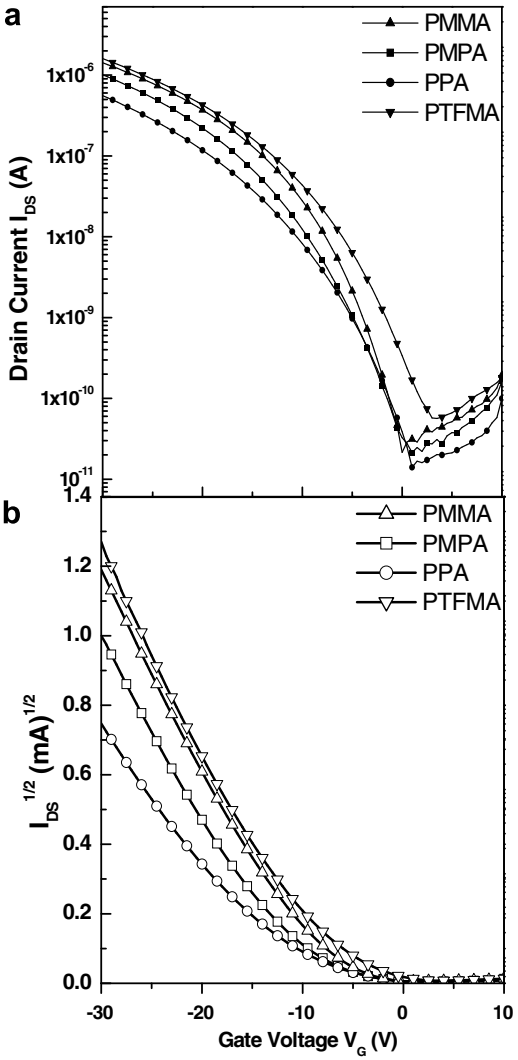

Fig. 4. Transfer characteristics of OTFTs with various gate dielectric materials. The gate voltage is swept at a constant drain-source voltage $V_{DS} = -30$ V.

features of drain-source current curves with PMMA gate dielectrics, and these devices mentioned above show higher saturation I_{DS} than that of PMPA and PPA at $V_{GS} = -30$ V.

The transfer characteristics of the devices are measured in the saturation region ($|V_{DS}| = 30\ \text{V} \geqslant |V_{GS}-V_{Th}|$), and representative transfer plots are shown in Fig. 4. The carrier mobility (μ_{sat}) and threshold voltage (V_T) are calculated from the slop and intercept of the linear part of the ($I_{DS}^{1/2}-V_G$) plot by fitting the data to Eq. (2) [27]:

$$\mu_{sat} = (2I_{DS}L)/[WC_i(V_G - V_{Th})], \quad (2)$$

where I_{DS}, L, W, C_i, V_G, and V_{Th} are the drain saturation current, channel length, channel width, gate dielectric capacitance, gate voltage, and threshold voltage, respectively. All parameters related to transfer characteristics are summarized in Table 2.

In this study, the observed charge-carrier mobility depends not only on the dielectric surface chemical characteristics but also on the dipole moment of the terminal groups on the dielectric side-chain. As shown in Table 2, gate insulators, with low surface energy and high dielectric constants, show a tendency to have high mobility due to the uniform pentacene thin-film phase and good crystallographic structure. Accordingly, PMMA and PMPA have similar dielectric constants and surface free energies. They also show similar topography with layer-by-layer crystal growing mode in AFM images (Fig. 2). Furthermore, their corresponding field-effect mobilities at the saturation region (μ_{sat}) are similar and measured at 0.153 $cm^2\ V^{-1}\ s^{-1}$ for PMMA and 0.134 $cm^2\ V^{-1}\ s^{-1}$for PMPA. In general, pentacene films grown in the layer-by-layer mode exhibit large grain sizes and relatively similar mobilities (e.g., PMMA and PMPA), but smaller grain sizes and poor mobilities in the island mode. However, pentacene film with the island mode growth in PTFMA device affords different OTFT characteristics ($\mu_{sat} = 0.195\ cm^2\ V^{-1}\ s^{-1}$) from that of the layer-by-layer mode. Thus, the field-effect mobility is relatively dropped when the thin-film phase and the single crystal phase synchronously grow and coexisted during thermal evaporation.[28]. Evidently, the topographies of PTFMA show the single crystal phase in Fig. 2. Hence, the PTFMA device has higher field-effect mobility than that of PMMA and PMPA.

The device characteristics of pentacene TFT based on different gate dielectrics are shown in Fig. 4a; the source-drain current I_{DS} in a logarithmic scale are shown against the gate voltage V_G at a constant source-drain voltage of $V_{DS} = -30$ V. All of these devices exhibit I_{on}/I_{off} values of four orders of magnitude and also show that I_{DS} values depend on the nature of polyacrylates. The I_{DS} value at $V_G = 0$ V is enhanced by one order of magnitude in devices with PTFMA compared with that of PMMA, indicating that

Table 2
Summary of the electrical performance parameter for OTFTs with different gate dielectrics

Dielectric	Mobility (μ_{sat} $cm^2\ V^{-1}\ s^{-1}$)	Capacitance (C_i; nF cm^{-2})	On–off current ratio (I_{on}/I_{off})	Turn-on voltage (V_{to}; V)	Threshold voltage (V_{Th}; V)	Dipole moment (D; Debye) [30]
PMMA	0.153	5.06	6.64×10^4	0.0	−7.03	0.94[a]
PMPA	0.134	4.56	4.72×10^4	1.0	−6.03	1.36[b]
PPA	0.093	4.41	3.97×10^4	1.0	−8.24	1.16[c]
PTFMA	0.195	5.35	2.83×10^4	3.5	−8.62	2.54[d]

Note: the side-chain group.
[a] Alkyl group ($-OCH_3$).
[b] Alkoxyaryl ($-OC_6H_5OCH_3$).
[c] Phenyl group ($-OC_6H_5$).
[d] Fluoroalkyl group ($-OCH_2CF_3$).

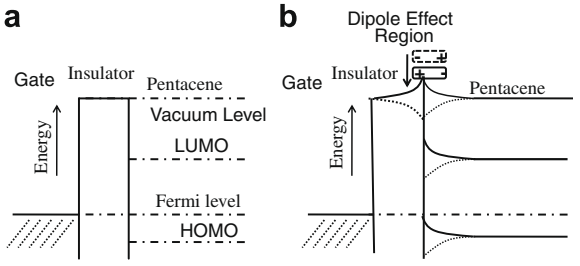

Fig. 5. Schematic energy level diagram for illustrating the interface between gate insulators and pentacene: (a) without and (b) with dipole effect between gate dielectric/pentacene interface. The "+" and "−" denote the hole and the electron, respectively.

the surface carrier is modulated by changing the terminal ester group on gate dielectrics.

The $I_{DS}^{1/2}$–V_G relations for devices are plotted in Fig. 4b. Through a linear fit for $I_{DS}^{1/2}$–V_G curves, we are able to estimate V_{Th} and μ_{sat} in the saturation region. Of particular interest is the change in V_{Th} with various polyacrylates. V_{Th} and V_{to} shift positive as dielectrics go from PPA through PMMA to PTFMA.

The observed V_{Th} and V_{to} shift correlates to the electron affinity of the polymeric insulators end group. The dipole structures synchronously form a built-in dipole-dipole field, and the induced field is equivalent to a gate voltage applied in the transistor channel. The electronegativity of the terminal functional group on polymeric dielectrics influences the charge distribution within the gate insulator and pentacene. This can lead to the formation of an electric dipole within the dielectric/pentacene interface. The field induced phenomenon was also studied by Campbell et al. [29], who proposed the charge distribution within similar molecules and found a dipole moment whose strength significantly depended on the functional group of the investigated molecules. In this presented circumstance, the electron affinity of a close-packed organized organic monolayer can differ from the properties of the isolated molecules. As a result, the charge density at the insulator-organic semiconductor interface has been organized in advance so that it would affect device performance dramatically. The change in surface potentially modifies interface properties, as illustrated in the schematic band diagram shown in Fig. 5. When pentacene is deposited onto a dielectric layer without the dipole effect, the vacuum levels are aligned and no bending of the HOMO and LUMO level occurs, as shown in Fig. 5a. When a negative gate voltage is applied, the Fermi level of the gate electrode shifts towards higher (electron) energies. A part of the applied gate voltage is dropped across the gate insulator, and since the band alignment of the HOMO and LUMO level is fixed with respect to the vacuum level, the remaining gate voltage bends HOMO and LUMO levels. As a result, mobile charge carriers can be accumulated and formed in the conducting channel. For a polymeric dielectric with a permanent dipole field inserted between the gate electrode and the pentacene, as shown in Fig. 5b, the dipole field of the polymeric insulator modifies the surface potential which has the same effect as applying a (negative) gate voltage. For a p-type OTFT, therefore, V_{Th} and V_{to} will shift to more a positive region when a polymer with high dipole moment is used as a gate dielectric layer.

4. Conclusion

We have demonstrated that the single-layered polyacrylate with electronegative side groups significantly induces a built-in field within the semiconductor/dielectrics interface in p-type organic TFTs. This built-in field also shifts both threshold voltage (V_{Th}) and turn-on voltage (V_{to}) to positive bias voltage in pentacene-based devices with increasing the dipole moment of the dielectric. Although SAMs approach was also employed as gate dielectrics and the ultrathin monolayer less than 10 nm would be effective for reducing the operational voltage, it would be a technical challenge for making a pin-hole free monolayer film in a large area. Accordingly, we find that our study provides a simple way of controlling channel charge density at very low density levels and consequently the V_{Th} value, which should be useful for fabricating OTFTs with improved functionality. Permittivity tunable polymeric dielectrics are also a promising route to alternative SAM processed, and they will also open up exciting possibilities for fabrication of large area TFT devices by inkjet printing.

Acknowledgement

This work was supported by the MOE ATU Program "Aim for the Top University" # 97W802 and NSC-96-2628-E009-021-MY3.

References

[1] F. Ebisawa, T. Kurokawa, S. Nara, J. Appl. Phys. 54 (1983) 3255.
[2] A. Tsumura, H. Koezuka, T. Ando, Appl. Phys. Lett. 49 (1986) 1210.
[3] A. Assadi, S. Svensson, M. Willander, O. Inganas, Appl. Phys. Lett. 53 (1988) 195.
[4] K. Kudo, M. Yamashina, T. Moriizumi, Jpn. J. Appl. Phys. 23 (1984) 30.
[5] G. Horowitz, D. Fichou, X.Z. Peng, Z.G. Xu, F. Garnier, Solid State Commun. 72 (1989) 381.
[6] H.E.A. Huitema, G.H. Gelinck, J.B.P.H. van der Putten, K.E. Kuijk, C.M. Hart, E. Cantatore, P.T. Herwig, A.J.J.M. van Breemen, D.M. de Leeuw, Nature 414 (2002) 99.
[7] C.D. Sheraw, L. Zhou, J.R. Huang, D.J. Gundlach, T.N. Jackson, M.G. Kane, I.G. Hill, M.S. Hammond, J. Campi, B.K. Greening, J. Francl, J. West, Appl. Phys. Lett. 80 (2002) 1088.
[8] C. Bartic, A. Campitelli, S. Borghs, Appl. Phys. Lett. 82 (2003) 475.
[9] B. Crone, A. Dodabalapur, Y.Y. Lin, R.W. Filas, Z. Bao, A. LaDuca, R. Sarpeshkar, H.E. Katz, W. Li, Nature 403 (2000) 521.
[10] H. Klauk, M. Halik, U. Zschieschang, F. Eder, G. Schmid, C. Dehm, Appl. Phys. Lett. 82 (2003) 4175.
[11] S. Kobayashi, T. Nishikawa, T. Takenobu, S. Mori, T. Shimoda, T. Mitani, H. Shimotani, N. Yoshimoto, S. Ogawa, Y. Iwasa, Nature Mater. 3 (2004) 317.
[12] K.P. Pernstich, S. Haas, D. Oberhoff, C. Goldmann, D.J. Gundlach, B. Batlogg, A.N. Rashid, G. Schitter, J. Appl. Phys. 96 (2004) 6431.
[13] D.L. Keyes, R.R. Lamonte, D. McNally, M. Bitritto, Photonics Spectra 30 (2001) 131–134.
[14] T.-S. Huang, Y.-K. Su, P.-C. Wang, Appl. Phys. Lett. 91 (2007) 92116.
[15] G.-W. Kang, K.-M. Park, J.-H. Song, C.H. Lee, D.H. Hwang, Curr. Appl. Phys. 5 (2005) 297.
[16] C.-S. Chuang, S.-T. Tsai, Y.-S. Lin, F.-C. Chen, H.-P.D. Shieh, Jpn. J. Appl. Phys. 46 (2007) L1197.
[17] K. Müller, I. Paloumpa, K. Henkel, D. Schmeißer, Mater. Sci. Eng. 26 (2006) 1028.
[18] D.-J. Liaw, R.-S. Lin, J. Macro. Sci. Part A 31 (1994) 715.
[19] B.S.R. Reddy, J. Poly. Mater. 16 (1999) 271.
[20] M. Raihane, B. Ameduri, J. Fluorine Chem. 127 (2006) 391.

[21] I. Kymissis, C.D. Dimitrakopoulos, S. Purushothaman, IEEE Trans. Electron Dev. 48 (2001) 1060–1064.
[22] M. Gindl, G. Sinn, W. Gindl, A. Reiterer, S. Tschegg, Colloids Surf. A: Physicochem. Eng. Aspects 181 (2001) 279.
[23] D.L. Smith, Thin-Film Deposition: Principles and Practice, McGraw-Hill, New York, 1995 (Chapter 5).
[24] C. Mattheus, J. Baas, A. Meetsma, J.L. de Boer, C. Kloc, T. Segrist, T.M. Palstra, Acta Crystallogr. E58 (2002) o1229.
[25] W.Y. Chou, C.W. Kuo, H.L. Cheng, Y.R. Chen, F.C. Tang, F.Y. Yang, D.Y. Shu, C.C. Liao, Appl. Phys. Lett. 89 (2006) 112126.
[26] J.E. Northrup, M.L. Tiago, S.G. Louie, Phys. Rev. B Phys. 66 (2002) 121404.
[27] S.M. Sze, Semiconductor Devices, Wiley, New York, 1985 (Chapter 5).
[28] C.D. Dimitrakopoulos, A.R. Brown, A. Pomp, J. Appl. Phys. 80 (1996) 2501.
[29] I.H. Campbell, S. Rubin, T.A. Zawodzinski, J.D. Kress, R.L. Martin, D.L. Smith, N.N. Barashkov, J.P. Ferraris, Phys. Rev. B 54 (1996) 4321.
[30] G.W. Gokel, Dean's Handbook of Organic Chemistry, second ed., McGraw-Hill, USA, 2004.